Accepted manuscript, 2019 – International Journal of Numerical Methods for Heat & Fluid Flow
Published version available online at: https://doi.org/10.1108/HFF-09-2018-0497

Strong fluid-solid interactions with segregated CFD solvers

Mathieu Olivier*, Olivier Paré-Lambert

Laboratoire de Mécanique des Fluides Numérique,
Department of Mechanical Engineering,
Faculty of Science and Engineering,
Université Laval, Quebec City, Quebec, G1V 0A6, Canada

Abstract

Purpose: A fluid-structure coupling partitioned scheme involving rigid bodies supported by spring-damper systems is presented. This scheme can be used with already existing fluid flow solvers without the need to modify them.

Design/methodology/approach: The scheme is based on a modified Broyden method. It solves the equations of solid body motion in which the external forces coming from the flow are provided by a segregated flow solver used as a black box. The whole scheme is implicit.

Findings: The proposed partitioned method is stable even in the ultimate case of very strong fluid-solid interactions involving a massless cylinder oscillating with no structural damping. The overhead associated with the coupling scheme represents an execution time increase by a factor of about 2 to 5, depending on the context. The scheme also has the advantage of being able to incorporate turbulence modeling directly through the flow solver. It has been tested successfully with URANS simulations without wall law, thus involving thin high aspect-ratio cells near the wall.

Originality/value: Such problems are known to be very difficult to solve and previous studies usually rely on monolithic approaches. To the authors' knowledge, this is the first time a partitioned scheme is used to solve fluid-solid interactions involving massless components.

Keywords: Fluid-structure interaction, partitioned approach, quasi-Newton methods, vortex induced vibrations

Paper type: Research paper.

1. Introduction

Fluid-Structure Interaction (FSI) problems are found in many fields of engineering and science. As a consequence, the development of numerical algorithms to solve such kind of problems has been largely active in the last two decades. The coupling algorithms found in literature are generally classified in two categories: loosely coupled schemes and tightly coupled schemes.

Loosely coupled schemes advance the solution in time by solving the solid and fluid fields sequentially. It follows that such schemes introduce some explicitness in the time integration scheme. For example, in the conventional staggered coupling algorithm of Piperno et al. (1995), the solid displacement is advanced in time by using the explicit fluid load from the previous time-step. Then, the geometry and the mesh of the fluid domain are updated, and the fluid solution is calculated before proceeding to the next time-step. Farhat and Lesoinne (2000) proposed an improved version of this algorithm that ensures second-order accuracy in time. A loosely coupled scheme can also be easily

*Corresponding author
Email addresses: mathieu.olivier@gmc.ulaval.ca (Mathieu Olivier), olivier.pare-lambert.1@ulaval.ca (Olivier Paré-Lambert)

Nomenclature

a	= discretization coefficient
$\mathbf{b}$	= discretization vector coefficient
c_i	= time scheme coefficient
$\mathbf{d}$	= displacement vector
(d_x, d_y)	= displacement vector components
D	= diameter of the cylinder
$\mathbf{F}$	= external fluid force vector
i	= iteration index
$\mathbf{I}$	= identity matrix
$\mathbf{J}$	= Jacobian matrix
k	= spring constant
k^*	= dimensionless spring constant
m	= mass of the cylinder
m^*	= dimensionless mass of the cylinder
n	= time index
$\mathbf{R}$	= residual vector
Re	= Reynolds number
t	= time
U_∞	= freestream velocity
U^*	= normalized velocity
$\mathbf{v}$	= velocity vector
w_i	= weight used in the modified Broyden method
y^+	= dimensionless wall distance
γ	= structural damping
γ^*	= dimensionless structural damping
Δt	= time-step
ζ	= damping ratio
ν	= kinematic viscosity
ρ	= fluid density

implemented by using explicit integration schemes in both the fluid and the solid domain. This strategy is well suited for compressible flows where the pressure or density equation can be marched in time (Persson et al., 2007) although stability conditions on the time-step size may become restrictive, justifying the need for a so-called implicit-explicit marching scheme (Froehle and Persson, 2014).

While loosely coupled schemes have been successfully applied to aeroelastic applications, they suffer from a added-mass instability that occurs when large fluid-to-solid density ratios are involved (Förster et al., 2007; Causin et al., 2005). In this context, tightly coupled algorithms, which can implement an implicit time marching scheme and enforce continuity of velocity and stress at the fluid-solid interface, can be used to ensure stability. Tightly coupled algorithms can be classified as either monolithic or partitioned schemes. Monolithic schemes consist in linearizing all discrete field equations and assembling a single linear system that accounts for all unknowns of the problem. Outer-iterations are needed only if the problem involves nonlinear equations. Monolithic schemes have been successfully implemented in various finite-element framework where, traditionally, nonlinear problems are solved in a coupled fashion (Hübner et al., 2004; Walhorn et al., 2005; Tezduyar et al., 2006; Hron and Turek, 2006). Such a monolithic implementation specialized for the fluid-solid interaction involving a rigid body was proposed recently along with the code verification that assesses the order of convergence of the method (Étienne and Pelletier, 2012; Yu et al., 2015). A similar implementation involving space-time finite elements is also proposed by Prakash Singh et al. (2013). On the other hand, partitioned schemes are based on the paradigm of using independent black-box solvers to manage respectively the fluid and the solid fields, while providing the ability to achieve formal implicit time-marching schemes by iterating between each solver at a given time. The partitioned approach has also been used in contexts that depart

from traditional finite-volume and finite-element frameworks. Applications of the approach with immersed-boundary methods (Bailoor et al., 2017) and smoothed profile method (Xie et al., 2017) has been successful. Although these developments are promising, it is the ability of the partitioned approach to be used with traditional fully-featured and well-tested tools that makes it attractive. However, even though the implicit partitioned approach is appealing, the stability problems of the loosely coupled scheme eventually occur, even if a fixed-point iteration procedure is used (Veilleux and Dumas, 2017). Recently, a coupling algorithm that introduces fictitious mass and damping in the solid equations was proposed and appeared to provide an efficient strategy to solve strongly coupled cases (Baek and Karniadakis, 2012; Deng et al., 2015).

This paper presents a fluid-solid coupling scheme based on Dirichlet-Neumann partitioning (i.e.: Dirichlet boundary conditions on the fluid side of the interface and Neumann-like boundary conditions on the solid side) that uses a finite-volume flow solver as a black box. In the present paper, the solid body is a rigid cylinder held by springs and dampers undergoing free oscillations in a flow. The proposed implicit two-way partitioned coupling algorithm is based on the modified Broyden method of Vanderbilt and Louie (1984). The resulting algorithm allows problems involving very strong fluid-solid interactions to be addressed without needing to specify fictitious mass and damping. The scheme, which can be classified in the quasi-Newton family (Vierendeels, 2006; Vierendeels et al., 2007; Degroote et al., 2009, 2010) is used with a segregated solution approach in the fluid solver, which, in turn, is both widespread in numerous CFD codes and efficient for transient problems. The ability of the coupling scheme to address strongly coupled FSI problems with a segregated CFD scheme allows an easy access to all features of the CFD solver (such as turbulence models) without needing modification to the code. The scope of the paper is thus to assess the performance of the proposed coupling scheme.

2. Governing equations and numerical methods

This work considers the interaction between a rigid cylinder mounted on two perpendicular spring-damper systems and an incompressible Newtonian fluid flow (see Fig. 1). The fluid flow is governed by the incompressible Navier-Stokes equations and the flow solver is based on the finite-volume method within the *OpenFOAM* library:

$$\nabla \cdot \mathbf{u} = 0,$$
$$\frac{\partial \mathbf{u}}{\partial t} + \mathbf{u} \cdot \nabla \mathbf{u} = -\frac{1}{\rho}\nabla p + \nu \nabla^2 \mathbf{u},$$

where ρ is the fluid density, ν is the fluid kinematic viscosity, p is the pressure field, $\mathbf{v}$ is the velocity field. The equations are implemented in an arbitrary Lagrangian-Eulerian formulation to account for the moving geometry. In the flow solver, the fluid-solid coupling is taken into account through the boundary condition at the cylinder where a standard moving-wall condition is used. This boundary condition provides the proper Dirichlet condition on the velocity field by considering the displacement of the mesh nodes which, in turn, comes from the solid displacement solution ($\mathbf{d}$). On the other hand, the motion of the cylinder is governed by a harmonic oscillator, which is given by:

$$m\frac{\partial^2 \mathbf{d}}{\partial t^2} + \gamma\frac{\partial \mathbf{d}}{\partial t} + k\mathbf{d} = \mathbf{F}, \tag{1}$$

where $\mathbf{d}$ is the displacement vector, m is the mass of the cylinder, γ is the structural damping, k is the spring constant, and $\mathbf{F}$ is the external fluid force coming from the flow solver that takes into account pressure and shear stresses on the whole cylinder wall. In order to provide more generality to the presented results, dimensionless parameters are used. A dimensional analysis of the problem provides the following four dimensionless parameters: the Reynolds number $Re = U_\infty D/\nu$, the mass ratio $m^* = 4m/(\pi\rho D^2)$, the dimensionless damping $\gamma^* = 2\gamma/(\rho U_\infty D)$, and the dimensionless stiffness $k^* = 2k/(\rho U_\infty^2)$. Note that in most studies involving vortex-induced vibration of cylinders, the dimensionless damping and the dimensionless stiffness are replaced by the reduced velocity and the damping ratio which can respectively be recovered with $U^* = \sqrt{2\pi^3 m^*/k^*}$ and $\zeta = \gamma^*/\sqrt{2\pi k^* m^*}$ (among others: Williamson and Govardhan (2004); Leontini et al. (2006)). Here, the former parameter set is preferred because it remains well definite when the cylinder mass is set to zero as pointed out by Shiels et al. (2001).

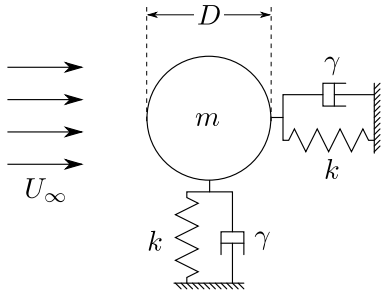

Figure 1: Problem setup: cylinder mounted on springs and dampers in a flow field.

The solid equation of motion (Eq. (1)) is discretized in time using the same implicit second-order backward differencing scheme as in the fluid discrete equations. By defining the velocity as $\mathbf{v} = \partial\mathbf{d}/\partial t$, it is possible to form two coupled first-order equations which can be reassembled after discretization to give the discrete solid equation in the form of the following residual $\mathbf{R}$:

$$\mathbf{R}(\mathbf{d}^{n+1}) = a\mathbf{d}^{n+1} + \mathbf{b} - \mathbf{F}^{n+1}(\mathbf{d}^{n+1}) = \mathbf{0}, \tag{2}$$

with:

$$a = mc_1^2 + \gamma c_1 + k, \tag{3}$$

$$\mathbf{b} = (mc_1c_2 + \gamma c_2)\mathbf{d}^n + (mc_1c_3 + \gamma c_3)\mathbf{d}^{n-1} + mc_2\mathbf{v}^n + mc_3\mathbf{v}^{n-1}. \tag{4}$$

In the case where the time-step Δt is kept constant, second-order backward differencing gives: $c_1 = 3/(2\Delta t)$, $c_2 = -2/\Delta t$, $c_3 = 1/(2\Delta t)$. The FSI coupling is taken into account on one hand, by considering the fluid force $\mathbf{F}$ as a source term in the solid equation (this is analogous to a Neumann boundary condition that would be needed in the case of a flexible solid, hence the Neumann-like designation used earlier), and, on the other hand, by applying the solid position and velocity in the fluid solver as a Dirichlet boundary condition. At each time-step, the whole FSI problem comes down to finding a vector $\mathbf{d}$ that satisfies Eq. (2). This is achieved by iterating both solvers in a fixed-point algorithm at each time-step since both the force acting on the cylinder and its velocity are not known until the solution at a given time has converged. The modified Broyden method described below is used to accelerate and stabilize this process.

In the special case where the structure would be moving along a single degree of freedom (e.g.: a cylinder undergoing transverse oscillation in a flow field while being retained in the flow direction), Eq. (2) would simply become $R(d_y) = 0$. Thus, for this simplified problem with a single degree-of-freedom, many classical methods for solving nonlinear equations can be used rather easily. Among these methods, the secant method has been tested and proved to be robust and efficient. Therefore, when more than a single degree of freedom is involved, the modified Broyden method proposed by Vanderbilt and Louie (1984), which is an improved version of the original method proposed by Broyden (1965), appears to be an interesting choice. Indeed, Broyden's method and its derivatives do not require the actual Jacobian matrix to be computed (either exactly or numerically) at every iteration, it simply updates it in a way that does not require extensive calls of the flow solver, which is very analogous to the secant method in 1-DOF problems. In the proposed algorithm, the initial Jacobian is approximated by a scaled identity matrix. In subsequent steps, the Jacobian is updated using a modified Broyden formula. The whole FSI algorithm is presented below (Algorithm 1) where the subscripts i represent the outer loop iteration index while the superscripts n represent the time index.

The first step of the algorithm is a predictor step in which a second-order Adams-Bashforth is used to predict the position of the solid body and the corresponding fluid fields. This step provides the first fluid-solid state used in the coupling scheme. The second step is the first quasi-Newton step in which the Jacobian matrix is guessed. Vanderbilt and Louie (1984) proposed to simply use the identity matrix $\mathbf{I}$ as an initial guess (this would correspond to $-\mathbf{I}$ in the present formulation). However, doing so leads to divergence of the algorithm in the present context. Dividing the identity matrix by the square of the weight w_2 provides a mean to under-relax the solution of the displacement

Algorithm 1 Fluid-solid coupling algorithm

1. First outer iteration ($i = 1$)
   (a) Prediction of the solid position (second-order explicit Adams-Bashforth scheme):
   $$\mathbf{d}_1^{n+1} = \mathbf{d}^n + \Delta t(3\mathbf{v}^n - \mathbf{v}^{n-1})/2.$$
   (b) Solution of the fluid flow to obtain $\mathbf{F}_1^{n+1}$ using $\mathbf{d}_1^{n+1}$ and $\mathbf{v}_1^{n+1}$ as a Dirichlet boundary condition.
2. Second outer iteration ($i = 2$, if needed)
   (a) Computation of the residual:
   $$\mathbf{R}_2 = a\mathbf{d}_1^{n+1} + \mathbf{b} - \mathbf{F}_1^{n+1}.$$
   (b) Jacobian matrix initial guess:
   $$\mathbf{J}_2 = \begin{bmatrix} -1/w_2^2 & 0 \\ 0 & -1/w_2^2 \end{bmatrix}.$$
   (c) Computation of the new solid position:
   $$\mathbf{d}_2^{n+1} = \mathbf{d}_1^{n+1} - (\mathbf{J}_2)^{-1} \cdot \mathbf{R}_2.$$
   (d) Solution of the fluid flow to obtain $\mathbf{F}_2^{n+1}$ using $\mathbf{d}_2^{n+1}$ and $\mathbf{v}_2^{n+1}$ as a Dirichlet boundary condition.
3. Subsequent outer iterations
   (a) Computation of the residual:
   $$\mathbf{R}_i = a\mathbf{d}_{i-1}^{n+1} + \mathbf{b} - \mathbf{F}_{i-1}^{n+1}.$$
   (b) Update of the Jacobian matrix using the modified Broyden method:
   $$\begin{aligned} \delta\mathbf{R}_i &= \mathbf{R}_i - \mathbf{R}_{i-1}, \\ \delta\mathbf{d}_{i-1} &= \mathbf{d}_{i-1} - \mathbf{d}_{i-2}, \\ \mathbf{B}_i &= w_2^2\mathbf{I} + \sum_{j=3}^{i} w_j^2 \left(\delta\mathbf{d}_{i-1} \otimes \delta\mathbf{d}_{i-1}\right), \\ \mathbf{G}_i &= w_2^2\mathbf{J_2} + \sum_{j=3}^{i} w_j^2 \left(\delta\mathbf{R}_{i-1} \otimes \delta\mathbf{d}_{i-1}\right), \\ \mathbf{J}_i &= \mathbf{G}_i \cdot \mathbf{B}_i^{-1}. \end{aligned}$$
   (c) Computation of the new solid position:
   $$\mathbf{d}_i^{n+1} = \mathbf{d}_{i-1}^{n+1} - (\mathbf{J}_i)^{-1} \cdot \mathbf{R}_i.$$
   (d) Solution of the fluid flow to obtain $\mathbf{F}_i^{n+1}$ using $\mathbf{d}_i^{n+1}$ and $\mathbf{v}_i^{n+1}$ as a Dirichlet boundary condition.
4. At convergence, increment time and return to step 1.

vector while remaining consistent with the algorithm formulation. In the present work, $w_2 = 0.005$ and $w_{i>2} = 1$ are used. These choices are arbitrary and provide a mean to tune the algorithm as pointed out by Vanderbilt and Louie (1984). Using a smaller weight on the initial Jacobian matrix, which is guessed, has the effect of reducing its impact in further Jacobian matrix updates. Moreover, since w_2^2 also acts as a relaxation factor for the displacement vector solution, it has a stabilizing effect on the iterative process. A small relaxation factor can then be interpreted as applying a small perturbation on the solution in order to estimate the Jacobian matrix afterward, which is common practice in Newton-like algorithms. Except for the first time-step of a simulation, it is possible to use the Jacobian matrix from the previous time-step as a good initial guess along with $w_2 = 1$. This strategy, which is used here, accelerates the convergence of the method since it allows at least one outer-iteration to be saved per time-step. Then,

the corresponding fluid fields are obtained by calling the flow solver and the subsequent steps of the algorithm can be carried out by updating the Jacobian matrix with the modified Broyden formulas (step 3).

Before presenting numerical results, it is worthwhile to highlight some remarks about the coupling algorithm. Firstly, in the algorithm, the flow solver does not need to be modified. However, to fully implement the proposed algorithm, the flow solver needs to be called more than once per time-step and it must be able to make the force on the solid surface available to an external code. In commercial "black-box" solvers, this is often possible through so-called user-defined functions. Moreover, Algorithm 1 has been arranged in a way where the flow solver is called at the end of each outer-iteration. Thereafter, the fluid force on the body can be computed and used by the solid solver on the next iteration. Calling the flow solver at the end of each outer-iteration allows the special treatments in the first two outer iterations to be easily managed within the solid module by using conditional statements.

Secondly, while the convergence rate of the modified Broyden method is not quadratic, it is still superlinear. As the results will show, the iterative process effectively takes only a few iterations to converge. Moreover, the fact that the convergence is not purely quadratic opens the door to performing partial solution of the fluid solver at each iteration without penalizing significantly the overall convergence rate, which reduces the computational effort at each outer iteration.

Thirdly, the predictor step (step 1a in Algorithm 1) is critical in the present incompressible flow context. Indeed, computing the first residual requires the fluid force acting on the body to be evaluated. The easiest way to do this is to compute the force by calling the fluid solver first in the coupling loop. However, this assumes that the solid body did not move since the last time-step which is, in a numerical perspective, equivalent to prescribing a sudden stop of the structure. In an incompressible flow context where the pressure field is strongly reactive to such shocks (because of the elliptic behavior of the pressure equation), this results in a force prediction that is, most of the time, very different from the actual solution and, as such, the latter is a poor initial guess to be used in the iterative process. Therefore, the prediction step is crucial for the convergence of the algorithm.

As a last remark, it was observed that, when the time-step is small enough, the predictor step produces a displacement vector very close to the actual solution such that the first computed $\delta\mathbf{d}$ and $\delta\mathbf{R}$ are very small. In these cases, the Jacobian matrix may become badly conditioned and the algorithm then becomes non-convergent. In the few cases where this behavior occured, the algorithm did not diverge, but it was unable to reach the specified tolerances. A simple cure was to either use a first-order predictor, which is less precise, or to reinitialize the Jacobian matrix (step 2) at each time-step.

3. Verification and validation

Verification and validation are performed by comparing the solution of a cylinder undergoing vortex-induced vibration with the results of Yang et al. (2008) and Blackburn and Karniadakis (1993). The simulations are performed with three levels of numerical resolution described in Table 1. The outer-loop iterations are run until the magnitude of the residual equations ($\|\mathbf{R}_i\|$) reaches a given tolerance. For the sake of the verification and validation, this tolerance is set to 1×10^{-9}, which was tested to be more than sufficient to prevent significant iteration errors in this case. Moreover, trying to reduce the residuals further is hardly possible because the ratio $\delta\mathbf{d}/\mathbf{d}$ often reaches machine precision. The domain used, which is the same as Yang et al. (2008), as well as the coarse mesh are presented in Fig. 2. The left side of the domain is an inlet boundary condition where the normal velocity is imposed as U_∞ along with a zero normal gradient for the pressure field. Top and bottom boundaries are assimilated as symmetry planes and a zero pressure along with a zero normal velocity gradient are applied on the right boundary (outlet). The parameters defining the problem are:

$$Re = 200, \quad m^* = 4/\pi, \gamma^* = 2\pi/125, \quad k^* = 8\pi^2/25.$$

The flow field is initialized with a potential flow solution around the cylinder that has been slightly moved to (0, $0.01D$) with respect to the original position depicted in Fig. 2 such that the spring is initially stretched. This initial offset acts as a perturbation that triggers the vortex street in a reproducible manner.

The trajectory of the cylinder for the last computed cycle is reported in Fig. 3. In this case, the motion of the cylinder reaches a periodic regime after some time. The results clearly indicate that the solution is convergent with respect to the numerical resolution and that the medium resolution is sufficient to capture the essential features of this problem. Moreover, the agreement with the trajectory reported by Blackburn and Karniadakis (1993) is very good. A

Table 1: Discretization used for the verification of the numerical method.

	Coarse	Medium	Fine
Number of cells	15065	65065	269140
Time-step $\Delta t\, U_\infty / D$	0.01	0.005	0.0025

slight offset of $\delta d_x/D = 0.002$ has been applied in order to match the center of the trajectory obtained by Blackburn and Karniadakis (1993) (Yang et al. (2008) used an offset of 0.0185).

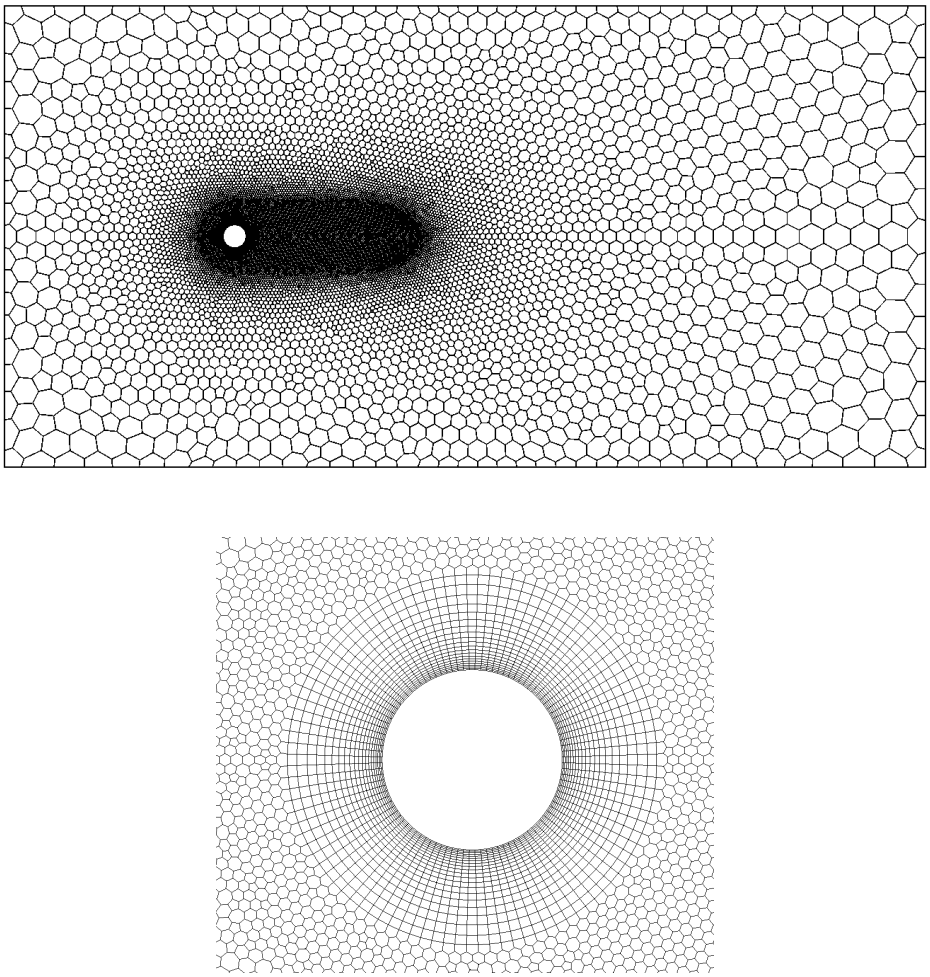

Figure 2: Coarse polyhedral mesh and domain dimensions.

4. Results and discussion

4.1. Coupling scheme performance

In order to assess the performance of the coupling scheme, the same numerical simulation is performed, but this time, the mass of the cylinder and the damping coefficient are both set to zero ($m = 0$, $\gamma = 0$). The dimensionless

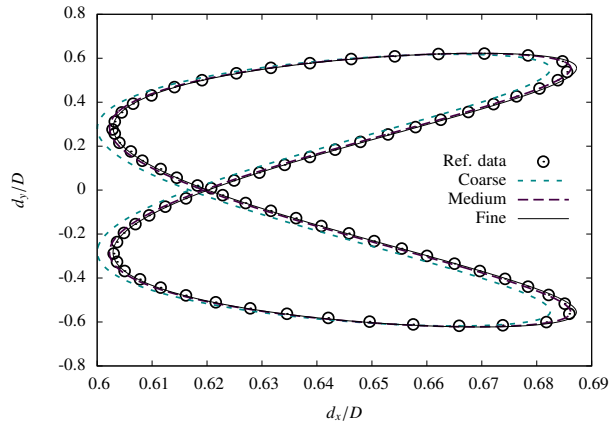

Figure 3: Cylinder trajectory of the last computed oscillation cycle with $Re = 200$, $m^* = 4/\pi$, $\gamma^* = 2\pi/125$, $k^* = 8\pi^2/25$. Different mesh resolutions are compared with the reference data of Blackburn and Karniadakis (1993).

parameters of the problem are then defined as:

$$Re = 200, \quad m^* = 0, \quad \gamma^* = 0, \quad k^* = 8\pi^2/25.$$

This scenario represents the limit case of strong fluid-solid interactions as the position of the cylinder is directly and solely governed by the fluid force ($\mathbf{d} = \mathbf{F}/k$). As such, the position of the cylinder must reach the equilibrium position of the spring on an instantaneous basis, without any lag effect produced by either inertia or damping. The simulation is performed with the medium resolution proposed in Table 1.

The cylinder trajectory obtained with this configuration is shown in Fig. 4. The results show that the motion of the cylinder reaches a quasi-periodic state since slight trajectory fluctuations from one cycle to another remain after $tU_\infty/D = 500$. The vorticity field corresponding to $tU_\infty/D = 500$ is presented in Fig. 5.

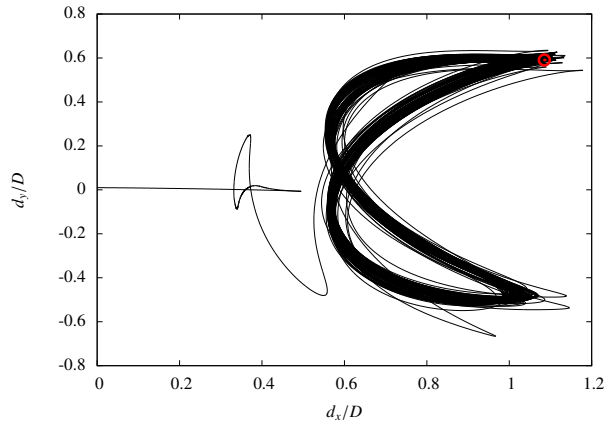

Figure 4: Trajectory of the cylinder with $Re = 200$, $m^* = 0$, $\gamma^* = 0$, and $k^* = 8\pi^2/25$. The red circle indicates the last computed time, i.e.: $tU_\infty/D = 500$.

In order to improve the numerical efficiency, the PIMPLE algorithm of the flow solver is tuned with the following configuration: at each flow solver call, 2 inner iterations are performed in which 3 pressure correction steps are used. It was found, by trial and error, that using more inner iterations does not improve the convergence rate of the coupling scheme. Indeed, the latter reaches the convergence criteria generally after 5 outer iterations. On the other

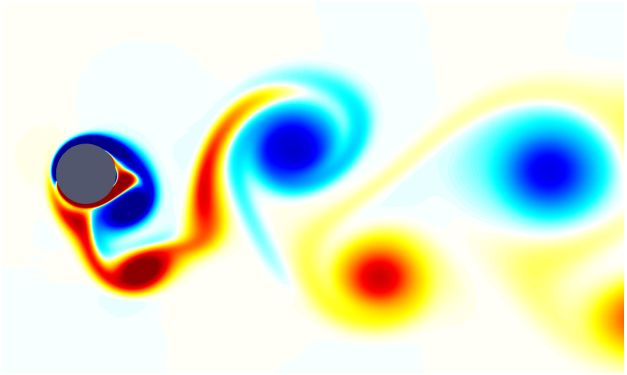

Figure 5: Vorticity field at $tU_\infty/D = 500$ with $Re = 200$, $m^* = 0$, $\gamma^* = 0$, and $k^* = 8\pi^2/25$.

hand, limiting the flow solver to only one inner iteration obviously makes each outer iteration faster, but the coupling scheme requires more iterations to converge which, in this case, slowed down the whole procedure.

The FSI simulation is then compared with a fluid-only simulation in which the motion of the cylinder is prescribed as $d_y = 0.5D\cos(0.4\pi tU_\infty/D)$ where the frequency corresponds to a Strouhal number of 0.2. This simulation is thus representative of the complexity of the fluid flow occurring in the FSI simulation. The configuration of the flow solver is the same as in the FSI simulation except that the number of inner iterations is determined by the convergence criteria and no outer iterations are required (i.e.: only one outer iteration is actually performed) since the flow solver is not coupled with any external module. Both simulations number of iterations and execution times are compared and reported in Table 2. It is observed that, even if the FSI simulation requires about 5 outer loops to converge (thus 5 fluid solver calls), the simulation time is only 2.13 times longer than the fluid-only simulation, thanks to the partial solutions at each outer loop. Lastly, the fact that the relative time of the FSI simulation is larger than the ratio of cumulative inner-loop iteration numbers (which is 1.43) is explained by intermediate mesh updates, FSI boundary conditions calculations, the solid solution (which is negligible here), and any other operation done by the black-box fluid solver between each call. Note that for cases with larger meshes, this difference is much less important (see Table 3 in the next section).

Table 2: Comparison of the computational cost of the FSI simulation with the imposed solid motion CFD simulation.

	Outer-loop iterations	Inner-loop iterations per time-step	Relative execution time
FSI	4.99	9.99	2.13
Imposed motion	1	7.00	1

4.2. A high Reynolds number case

The solution of a similar case with the same geometry, but with a higher Reynolds number is proposed. For this cases, the dimensionless parameters are:

$$Re = 10^5, \quad m^* = 0, \quad \gamma^* = 0, \quad k^* = 8.$$

To account for the turbulent nature of this configuration, the $k-\omega$ SST turbulence model (Menter and Esch, 2001; Menter et al., 2003) is used and the model is integrated up to the wall (thus, without a wall function). As such, an unstructured quadrilateral mesh with $y^+ < 1$ on the cylinder surface is used. A finer resolution is used to capture the main structures in the flow (boundary layer and wake vortices). A close-up view of the mesh near the cylinder is shown in Fig. 6. Here, a residual tolerance of 10^{-7} is used along with an adaptive time-stepping strategy. The time-step is such that the local Courant number remains below 0.85 everywhere in the mesh. This case therefore provides characteristics that are to be found in many engineering applications: an unstructured mesh (with 140 862 cells in

this case), thin high-aspect-ratio cells near the wall such that $y^+ < 1$, a wide spectrum of cell sizes, and a system of equation that is stiffer than those related to laminar flows. These characteristics make this case a good candidate to evaluate the applicability of the proposed algorithm to general CFD applications involving strong fluid-solid coupling.

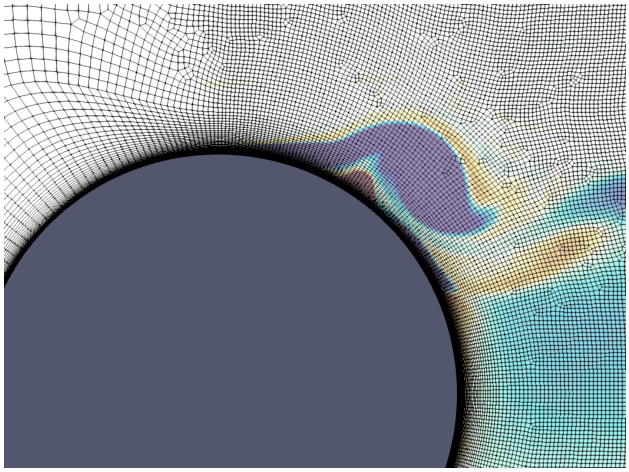

Figure 6: Mesh and vorticity field near the cylinder at $tU_\infty/D = 50$ with $Re = 10^5$, $m^* = 0$, $\gamma^* = 0$, and $k^* = 8$.

This time, at each call of the flow solver, stopping criteria based on relative residuals was used such that the residuals of each equation drop at least three orders of magnitude. The PIMPLE algorithm is used with 2 pressure correction steps along with solution under-relaxation. The relaxation factors are 0.65 for the momentum, k, and ω equations and 0.85 for the pressure correction. This solver configuration is less aggressive than the one used for the laminar cases above since the latter appeared to be unstable with the use of the turbulence model for this specific case. Using this configuration, the outer loop converges in 5-6 outer iterations in which the fluid solver undergoes about 10 iterations per call. While these numbers allow good convergence of the algorithm, the overhead associated with the fluid-solid coupling remains relatively high. Unfortunately, it was not possible to reduce the computational effort at each outer iteration further without impairing the outer loop convergence rate significantly. Nevertheless, the method proved to be stable and convergent even though the fluid-solid interaction is very strong.

The results of the turbulent case present a chaotic trajectory of the cylinder (Fig. 7). This is not surprising when recalling that the laminar case with the massless cylinder also exhibits irregularities, although not as strong as the turbulent case. Indeed, the different vortex scales found in the wake as well as their different frequencies certainly contribute to this unstable behavior (Fig. 8). However, even though it is not the scope of the present paper to analyze the physics at stake, it is worth pointing out that the interpretation of the instantaneous displacement curve is delicate in the context of URANS flow modeling.

Here again, a simulation involving an imposed motion on the cylinder is used to establish the fluid solver settings and to obtain a basis for comparison with the coupled simulation. The residual stopping criterion is now based on the pressure equation, which is usually the last quantity to converge in the segregated algorithm. The actual value of the pressure residual in the FSI simulation is not meaningful since the solid body moves between flow solver calls. Therefore, its actual value lies somewhere between the initial and the final residual value of the last flow solver call. In order to present a relatively fair comparison, the stopping criterion is thus set to 10^{-6}. The summary of the solver performances for both the FSI and flow-only simulations are shown in Table 3. In terms of execution time, the FSI simulation is 4.64 times longer than the flow-only simulation.

4.3. A three-dimensional case

Lastly, a three-dimensional numerical simulation is performed in order to assess further the performance of the FSI coupling scheme in a context of a complex fluid flow. For this simulation, the solid motion remains constrained in the xy plane such that there is no motion in the span direction. The same fluid-solid coupling scheme is thus used. Once again, a very strong fluid-solid interaction is considered. Though no turbulence modelling is used, a higher

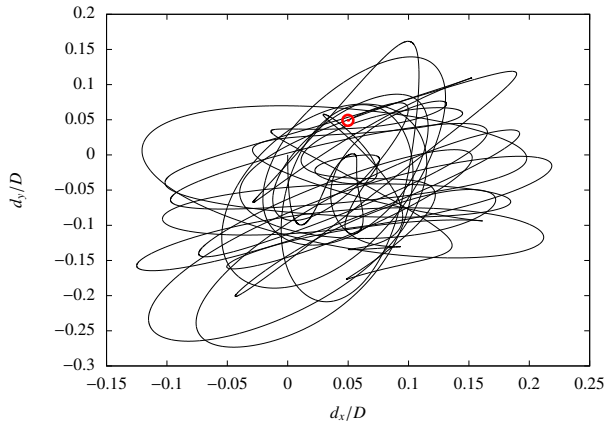

Figure 7: Trajectory of the cylinder with $Re = 1 \times 10^5$, $m^* = 0$, $\gamma^* = 0$, and $k^* = 8$. The red circle indicates the last computed time, i.e.: $tU_\infty/D = 50$.

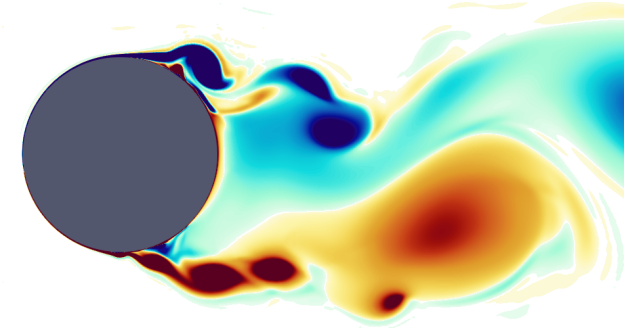

Figure 8: Vorticity field at $tU_\infty/D = 50$ with $Re = 10^5$, $m^* = 0$, $\gamma^* = 0$, and $k^* = 8$.

Reynolds number of 1000 is employed in order to provide a flow with three-dimensional unstable structures. The dimensionless parameters for this case are summarized as:

$$Re = 10^3, \quad m^* = 0, \quad \gamma^* = 0, \quad k^* = 8\pi^2/25.$$

A three-dimensional polyhedral mesh adopting the same domain dimensions as the one described in Fig. 2 is now used. The length of the domain in the span direction is $2D$ such that the resulting mesh is composed of 671 003 cells and symmetry boundary conditions are applied on both sides. The same time-stepping strategy is employed, however, the time-step is now kept such as the Courant number remains below 0.5 for all cells. The simulation is run until $tU_\infty/D = 200$ to ensure enough cycles and time-steps are carried out in order to compare results with the imposed motion case. The final instantaneous vorticity field is presented in Fig. 9. In this case, the outer loop usually converges in about 4 outer iterations in which the fluid solver undergoes about 4 iterations per call. Similarly to the turbulent case, this configuration also displays a chaotic trajectory of the cylinder. This is mainly caused by three-dimensional effects in the wake of the cylinder which are known to occur when the Reynolds numbers is higher than about 200 (Singh and Mittal, 2005). Fig. 9 shows some of these three-dimensional vortex structures in the wake, and demonstrates that the FSI coupling partitioned scheme proposed works as expected in a three-dimensional case.

Finally, Table 4 summarizes and compares the performances of the FSI coupling scheme with an imposed motion simulation using the same three-dimensional mesh. The prescribed amplitude for the imposed motion is set a little higher to account for greater amplitudes in the cylinder displacement with $Re = 1000$. The motion of the cylinder is therefore governed by $d_y = 0.7D\cos(0.4\pi tU_\infty/D)$ and the residual stopping criteria based on the pressure equation

Table 3: Comparison of the computational cost of the $k-\omega$ SST FSI simulation with the imposed solid motion CFD simulation.

	Outer-loop iterations	Inner-loop iterations per time-step	Relative execution time
FSI	5.65	57.1	4.64
Imposed motion	1	12.5	1

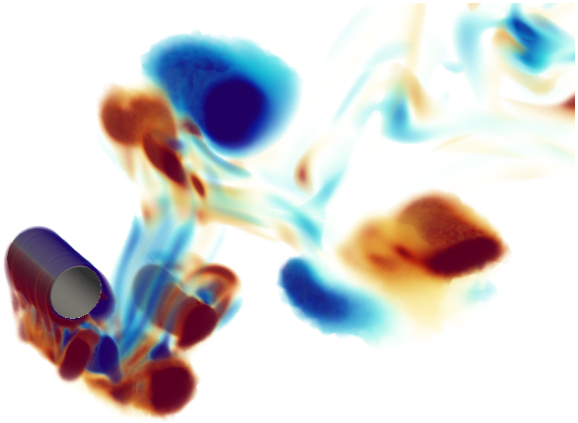

Figure 9: Vorticity field near the cylinder at $tU_\infty/D = 200$ with $Re = 10^3$, $m^* = 0$, $\gamma^* = 0$, and $k^* = 8\pi^2/25$.

stays at 10^{-6} in order to obtain a fair comparison. In this case, the ratio of execution time is 3.69, which is also acceptable considering that $m^* = 0$ and $\gamma^* = 0$.

Table 4: Comparison of the computational cost of the three-dimensional FSI simulation with the imposed solid motion CFD simulation.

	Outer-loop iterations	Inner-loop iterations per time-step	Relative execution time
FSI	3.93	15.7	3.69
Imposed motion	1	4.99	1

5. Concluding remarks

While strong fluid-solid interactions can be solved with a monolithic approach, the latter requires a fully-coupled treatment of all equations that include the degrees of freedom of the fluid field equations (including the turbulence model, if any), the solid equations, as well as moving mesh related degrees of freedom. In the context of transient simulations, segregated algorithms based on projection methods are known to be very efficient. The proposed FSI coupling scheme allows such algorithms to be used without excessive overhead while ensuring numerical stability. Moreover, the reported computational time increases (by a factor of about 2 to 5, depending on the context) correspond to the limit case where both the mass of the moving body and the structural damping are zero. For instance, increasing the mass of the body has the effect of reducing the strength of the interaction which results in a faster convergence of the scheme.

In the present model, the solid body equations of motion are uncoupled linear equations. Therefore, the nonlinearity and the coupling terms (that are responsible for the off-diagonal terms in the Jacobian matrix) originate solely from the flow. Future work will consider component-coupled nonlinear solid-body motion equations as well as application to more complex flows. Application to cases involving more than two structural degrees of freedom will also be considered.

References

Baek, H. and Karniadakis, G. E. (2012), 'A convergence study of a new partitioned fluid-structure interaction algorithm based on fictitious mass and damping', *Journal of Computational Physics* **231**, 629–652.

Bailoor, S., Annangi, A., Seo, J. H. and Bhardwaj, R. (2017), 'Fluid–structure interaction solver for compressible flows with applications to blast loading on thin elastic structures', *Applied Mathematical Modelling* **52**, 470 – 492.

Blackburn, H. and Karniadakis, G. (1993), Two-and three-dimensional simulations of vortex-induced vibration or a circular cylinder, *in* 'The Third International Offshore and Polar Engineering Conference, vol. 3', Singapore.

Broyden, C. G. (1965), 'A Class of Methods for Solving Nonlinear Simultaneous Equations', *Mathematics of Computation* **19**, 577–593.

Causin, P., Gerbeau, J. and Nobile, F. (2005), 'Added-mass effect in the design of partitioned algorithms for fluid-structure problems', *Computer Methods in Applied Mechanics and Engineering* **194**, 4506–4527.

Degroote, J., Bathe, J. and Vierendeels, J. (2009), 'Performance of a new partitioned procedure versus a monolithic procedure in fluid-structure interaction', *Computers and Structures* **87**, 793–801.

Degroote, J., Haelterman, R., Annerel, S., Bruggeman, P. and Vierendeels, J. (2010), 'Performance of partitioned procedures in fluid–structure interaction', *Computers and Structures* **88**(7–8), 446 – 457.

Deng, J., Teng, L., Pan, D. and Shao, X. (2015), 'Inertial effects of the semi-passive flapping foil on its energy extraction efficiency', *Physics of Fluids* **27**(5).

Étienne, S. and Pelletier, D. (2012), 'The low Reynolds number limit of vortex-induced vibrations', *Journal of Fluids and Structures* **31**, 18–29.

Farhat, C. and Lesoinne, M. (2000), 'Two efficient staggered algorithms for the serial and parallel solution of three-dimensional nonlinear transient aeroelastic problems', *Computer Methods in Applied Mechanics and Engineering* **182**, 499–515.

Förster, C., Wall, W. and Ramm, E. (2007), 'Artificial added mass instabilities in sequential staggered coupling of nonlinear structures and incompressible viscous flows', *Computer Methods in Applied Mechanics and Engineering* **196**(7), 1278 – 1293.

Froehle, B. and Persson, P.-O. (2014), 'A high-order discontinuous galerkin method for fluid–structure interaction with efficient implicit–explicit time stepping', *Journal of Computational Physics* **272**, 455 – 470.

Hron, J. and Turek, S. (2006), A monolithic fem/multigrid solver for an ale formulation of fluid-structure interaction with applications in biomechanics, *in* H. Bungartz, M. Schäfer, T. Barth, M. Griebel, D. Keyes, R. Nieminen, D. Roose and T. Schlick, eds, 'Fluid-Structure Interaction', Vol. 53 of *Lecture Notes in Computational Science and Engineering*, Springer Berlin Heidelberg, pp. 146–170.

Hübner, B., Walhorn, E. and Dinkler, D. (2004), 'A monolithic approach to fluid-structure interaction using space-time finite elements', *Computer Methods in Applied Mechanics and Engineering* **193**, 2087–2104.

Leontini, J., Thompson, M. and Hourigan, K. (2006), 'The beginning of branching behaviour of vortex-induced vibration during two-dimensional flow', *Journal of Fluids and Structures* **22**(6–7), 857 – 864.

Menter, F. and Esch, T. (2001), Elements of industrial heat transfer predictions, *in* '16th Brazilian Congress Of Mechanical Engineering'.

Menter, F. R., Kuntz, M. and Langtry, R. (2003), Ten Years of Industrial Experience with the SST Turbulence Model, *in* K. Hanjalić et al., eds, 'Fourth International Symposium on Turbulence, Heat and Mass Transfer', Begell House, Antalya, pp. 625 – 632.

Persson, P.-O., Peraire, J. and Bonet, J. (2007), A high order discontinuous galerkin method for fluid-structure interaction, *in* '18th AIAA Computational Fluid Dynamics Conference', p. 4327.

Piperno, S., Farhat, C. and Larrouturou, B. (1995), 'Partitioned procedures for the transient solution of coupled aroelastic problems Part I: Model problem, theory and two-dimensional application', *Computer Methods in Applied Mechanics and Engineering* **124**(1–2), 79 – 112.

Prakash Singh, S., Biswas, G. and Nithiarasu, P. (2013), 'A numerical study of vortex shedding from a circular cylinder vibrating in the in-line direction', *International Journal of Numerical Methods for Heat & Fluid Flow* **23**(8), 1449–1462.

Shiels, D., Leonard, A. and Roshko, A. (2001), 'Flow-induced vibration of a circular cylinder at limiting structural parameters', *Journal of Fluids and Structures* **15**, 3–21.

Singh, S. and Mittal, S. (2005), 'Vortex-induced oscillations at low reynolds numbers: Hysteresis and vortex-shedding modes', *Journal of Fluids and Structures* **20**(8), 1085 – 1104.

Tezduyar, T., Sathe, S., Keedy, R. and Stein, K. (2006), 'Space-time finite element techniques for computation of fluid-structure interactions', *Computer Methods in Applied Mechanics and Engineering* **195**, 2002–2027.

Vanderbilt, D. and Louie, S. G. (1984), 'Total energies of diamond (111) surface reconstructions by a linear combination of atomic orbitals method', *Physical Review B* **30**(10), 6118–6130.

Veilleux, J.-C. and Dumas, G. (2017), 'Numerical optimization of a fully-passive flapping-airfoil turbine', *Journal of Fluids and Structures* **70**, 102–130.

Vierendeels, J. (2006), Implicit coupling of partitioned fluid-structure interaction solvers using reduced-order models, *in* H. Bungartz et al., eds, 'Fluid-Structure Interaction', Vol. 53 of *Lecture Notes in Computational Science and Engineering*, Springer Berlin Heidelberg, pp. 1–18.

Vierendeels, J., Lanoye, L., Degroote, J. and Verdonck, P. (2007), 'Implicit coupling of partitioned fluid–structure interaction problems with reduced order models', *Computers and Structures* **85**(11–14), 970 – 976. Fourth MIT Conference on Computational Fluid and Solid Mechanics.

Walhorn, E., Kölke, A., Hübner, B. and Dinkler, D. (2005), 'Fluid-structure coupling within a monolithic model involving free surface flow', *Computers and Structures* **83**, 2100–2111.

Williamson, C. and Govardhan, R. (2004), 'Vortex-induced vibrations', *Annual Review of Fluid Mechanics* **36**, 413–455.

Xie, F., Pan, D., Zheng, Y. and Zou, J. (2017), 'Smoothed profile method and its applications in VIV', *International Journal of Numerical Methods for Heat & Fluid Flow* **27**(7), 1623–1635.

Yang, J., Preidikman, S. and Balaras, E. (2008), 'A strongly coupled, embedded-boundary method for fluid–structure interactions of elastically mounted rigid bodies', *Journal of Fluids and Structures* **24**(2), 167 – 182.

Yu, K. R., Étienne, S., Hay, A. and Pelletier, D. (2015), 'Code verification for unsteady 3-D fluid–solid interaction problems', *Theoretical and Computational Fluid Dynamics* **29**(5-6), 455–471.